Letter

Probing the Polysulfide Confinement in Two Different Sulfur Hosts for a Mg|S Battery Employing Operando Raman and Ex-Situ UV–Visible Spectroscopy

Ravindra Kumar Bhardwaj,[#] Ruth Gomes,[#] and Aninda J. Bhattacharyya*

Read Online

ACCESS | Metrics & More | Article Recommendations | SI Supporting Information

ABSTRACT: We study here the Mg-polysulfide confinement inside two structurally different model porous materials, viz., toray carbon paper (TC) and multiwalled carbon nanotubes (CNT), using operando Raman and postcycling ex-situ UV–vis spectroscopy. Sulfur encapsulated inside CNT (CNT-S) and TC (TC-S) serves as S-cathodes in a rechargeable room temperature Mg|S battery. Operando Raman spectroscopy indicates the presence of higher-order Mg-polysulfides at the CNT cathode. This is due to the combination of their entrapment inside CNT and also possibly to their localization in the liquid electrolyte in the vicinity of CNT-S. This finding is directly correlated to the ex-situ UV–vis spectroscopy, which shows a lesser degree of Mg-polysulfide dissolution into the electrolyte solution. In comparison, TC-S, where sulfur is encapsulated within the open matrix formed by the nanofiber network of the carbon paper, displays poorer polysulfide confinement. The distinct differences in their abilities to confine the Mg-polysulfides are corroborated by battery performance. In the current density range (0.05−1) C, the battery with CNT-S displays much higher specific capacities, being nearly two times that of TC-S at 1 C.
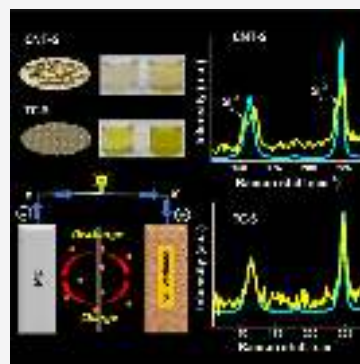
There is a great necessity for reliable rechargeable batteries in electric vehicles and grid storage.[1] As these large-scale applications will be used across diverse national economies in humongous numbers, the vastly successful Li-ion battery will eventually not suffice in meeting the stringent requirements in terms of cost, safety, and performance.[2−5] It has become imperative to explore electrochemical storage beyond the Li-ion or Li-based chemistry.[6−8] Magnesium (Mg), which is the fifth most abundant element in the Earth's crust and nearly 30 times cheaper than Li, offers great opportunities for the development of low cost, safe, and sustainable batteries.[9−12] The combination of the Mg anode with sulfur cathode will not only further reduce the cost but will also provide a higher performing battery (theoretical volumetric energy density = 3200 Wh L^{-1}), compared to even the advanced Li-ion. Despite this potential, the complexities of Mg-based chemistry pose several hurdles toward the development of suitable Mg-electrolytes and electrodes.[13−16] In addition, dissolution of polysulfides into the liquid electrolyte, which transcends across various metal−sulfur chemistries, persists as a challenge impeding the success of Mg|S batteries.[17−21] In this scenario, fundamental insights into confinement mechanisms, polysulfide intermediates, and associated electrochemical phenomena become important for the development of stable Mg|S batteries.[22−25] In this work, we focus on this aspect and demonstrate the efficacy of operando Raman spectroscopy to account for the mechanisms of polysulfide entrapment inside two morphologically different but well-known and widely used

commercial porous carbonaceous hosts, viz., multiwalled carbon nanotubes and porous carbon paper. Furthermore, the findings from operando Raman are convincingly supported via postcycling ex-situ UV−vis spectroscopy of the electrolyte solution. This investigative study on well-known matrices identifies the crucial structural parameters necessary for the design of new S-host or S-cathode configurations with high polysulfide trapping efficiency effectively resulting in a stable Mg|S battery.

The two S-hosts, viz., multiwalled carbon nanotube (CNT) and toray carbon (TC) paper and the subsequent S-encapsulation inside them, are described in section S1 and Figure 1. In comparison to the CNT-S sample, the powder X-ray diffraction (PXRD) peaks corresponding to sulfur for the TC-S are more prominent (Figure 2a). Figure S1 shows the XRD of CNT and TC. While in TC the sulfur particles are confined inside the pores (Figure 2c) formed by the randomly oriented nanofibers of the planar TC paper (Figure S2a), the sulfur is completely confined inside the open-ended CNT (Figure 2d and Figure S2b). The end opening of CNT is further confirmed by TEM analysis as shown in Figure S3. This
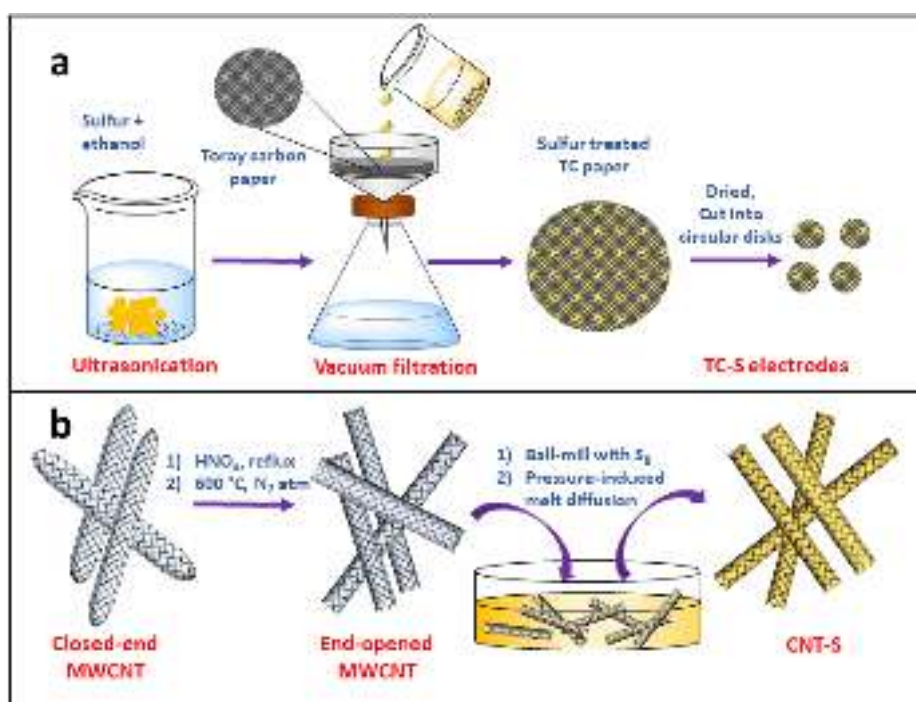
Figure 1. Schematic representation of preparation of (a) TC-S and (b) CNT-S cathode.
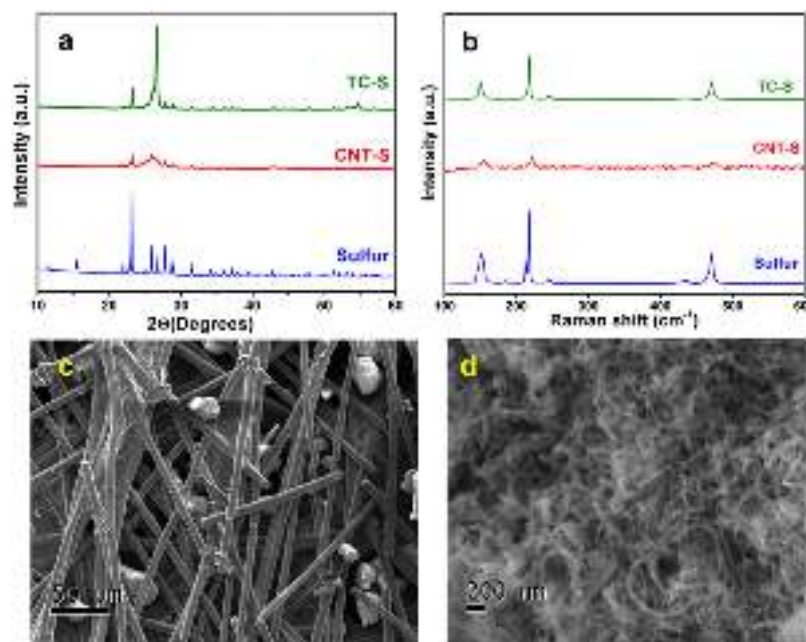

Figure 2. (a) X-ray diffraction patterns of elemental sulfur (blue), CNT-S (red), TC-S (green). (b) Raman spectra of the elemental sulfur (blue), CNT-S (red), TC-S (green). Scanning electron microscopy (SEM) image of (c) TC-S and (d) CNT-S.

is further confirmed by energy dispersive spectra (EDS) of CNT-S, which shows only 5.9% (w/w) of sulfur residing outside the open-ended CNT (Figure S4). In line with the PXRD and SEM results, the intensity of Raman bands for sulfur is much weaker in the case of CNT-S compared to that of TC-S (Figures 1b and S5b). The characteristic D and G bands in the Raman spectra of pure CNT and TC paper are shown in Figure S5a. This result confirms that the sulfur is predominantly confined inside the CNTs and should be more efficient than TC in confining S.

The implications of the morphological differences and their ensuing ability in confining sulfur are ascertained using operando Raman spectroscopy (cf. Supporting Information section S1 and Figure S6). The Raman spectra are collected at specific depths of the discharge voltage and at the end of a complete charge. Figure 3a,b shows the operando Raman spectra of the Mg|S cell with CNT-S and TC-S cathodes at various depths of discharge voltage. At OCV, both cathodes show bands at 157, 223, and 475 cm^{-1}. The first two bands are related to the bending modes, and latter is associated with the stretching mode of sulfur.[26−28] The intensities of the sulfur
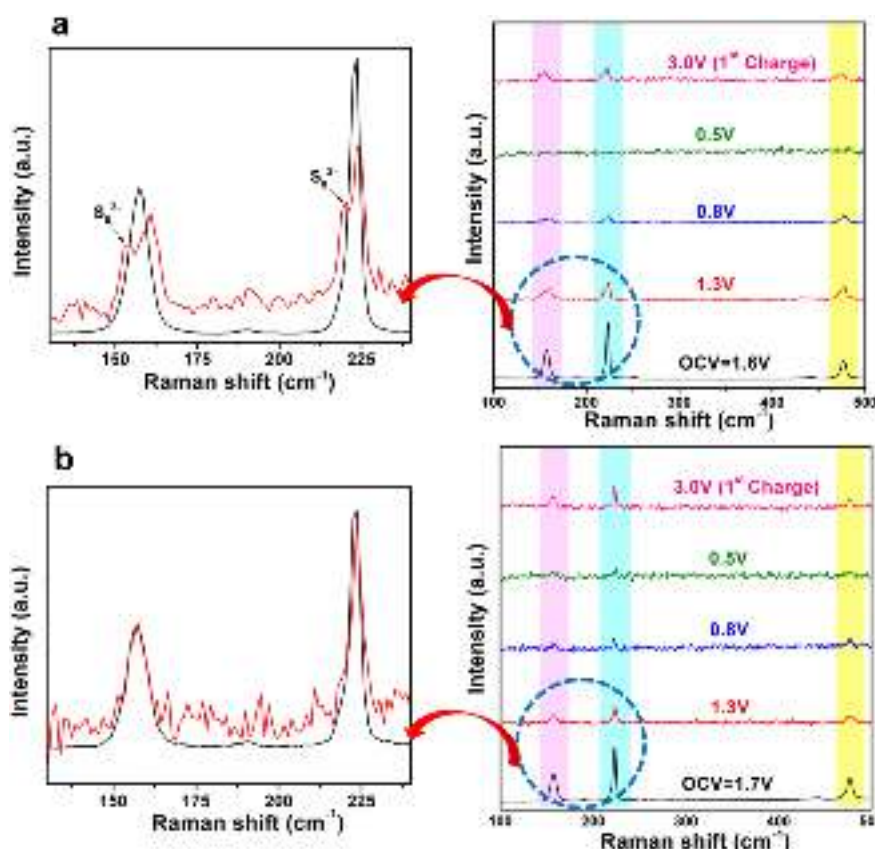
Figure 3. Operando Raman spectra of the Mg|S cell at different discharge voltages using (a) CNT-S and (b) TC-S. Magnified Raman spectra at 1.3 V (red) and OCV (black) for both cathodes are shown in the enlarged image.

bands are observed to decrease with an increase in the depth of discharge from 1.6 to 0.8 V and completely disappear at the discharge voltage of 0.5 V. The disappearance of the bands at 0.5 V is attributed to the conversion of sulfur to magnesium sulfide (MgS). During the charge, the reappearance of the S-bands is observed in both cathodes (Figure 3a,b, pink curves). Interestingly, a considerable broadening of the band at 157 and 223 cm^{-1} is observed at a discharge voltage of 1.3 V in the case of the CNT-S cathode (Figure 3a, red curve). On careful observation, as shown in the enlarged image of Figure 3a, two additional bands (humps) are observed at 153 and 219 cm^{-1}. The humps at 153 and 219 cm^{-1} are attributed to the presence of higher-order polysulfides, which confirms the confinement of higher-order polysulfides inside the carbon nanotubes of the CNT-S cathode. It is envisaged that the polysulfide trapping takes place partially via the interaction involving the sulfur of the metal polysulfide with that of remnant functional groups on the CNT and trapping in the defects in the stacking structure. The band splitting is not observed in the case of the TC-S cathode (Figure 3b, enlarged), which confirms that the entrapment of higher-order polysulfides does not take place or is considerably less in the case of the TC-S cathode. This is directly attributed to the inefficient confinement of the sulfur and polysulfides inside the TC-host. The operando Raman spectra for both of the cathodes at OCV shows Raman bands at 157, 223, and 475 cm^{-1} due to the presence of sulfur (Figure 3). This matches well with the Raman spectra of the CNT-S, TC-S, and elemental sulfur (as shown in Figure 1b). Following discharge to 1.3 V, it is observed that in the case of CNT-S, additional humps appear at 153 and 219 cm^{-1} (Figure 3a, enlarge area). This is attributed to the presence of higher-order

polysulfides. As the Raman measurement here has been done operando, there is an uncertainty in the exact ascertaining of the origin of such Raman signals. In the context of the methodology adopted here, it will be hard to differentiate whether the polysulfides are confined inside CNT or residing at the interface of the liquid electrolyte and the S-cathode. The occurrence of these humps only in the case of CNT-S strongly suggests that the concentration of polysulfides is higher, which can be due to a combination of polysulfides residing inside CNT and those residing in the liquid electrolyte in the immediate vicinity of the S-cathode. The absence of such humps near 153 and 219 cm^{-1} in TC-S strongly suggests higher dissolution in the case of TC. Unlike CNT, the TC is not as efficient in confining the higher-order polysulfides within the substrate nor restraining substantial amounts of polysulfides near to the S-cathode. Additionally, the humps observed near 153 and 219 cm^{-1} are not noise. They are also observed at a discharge voltage of 0.8 V in the case of the CNT-S cathode as shown in Figure S7 (blue curve in the expanded plot). Figure S8a,b shows the magnified Raman spectra of the 475 cm^{-1} bands for CNT-S and TC-S. No additional humps are observed in both cases. However, the changes in the band for TC-S occur at a faster rate than the CNT-S.

In line with literature reports on the Li|S battery employing operando Raman spectroscopy, our data are also unable to capture the bands exactly pertaining to the formation of MgS.[29−33] In spite of this, the Raman data convincingly confirm that the CNT-S cathode is more efficient in confining sulfur and intermediate polysulfides and results in a better battery performance in comparison to TC-S (vide infra).
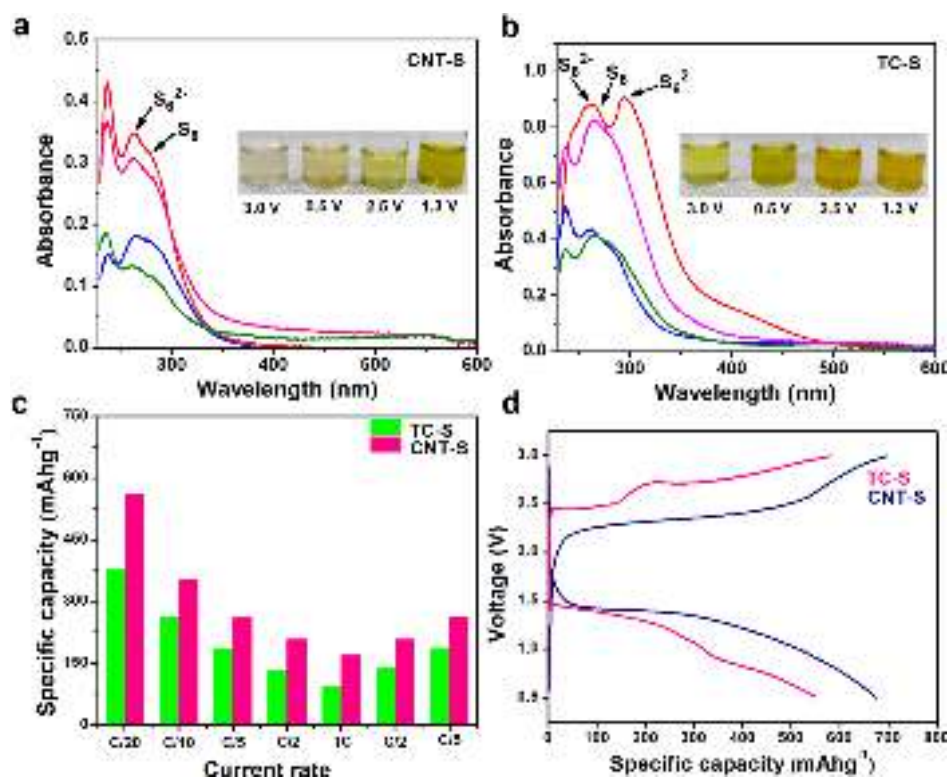
Figure 4. Comparative UV−visible spectra of the solutions at different discharge voltages of 1.3 V (red), 0.5 V (green), and charge voltage 2.5 V (pink), 3.0 V (blue) obtained after dilution (a) for the CNT-S cathode and (b) for the TC-S cathode (photographs of solutions obtained upon soaking the separators taken from cells after different charge/discharge voltage for CNT-S and TC-S cathodes are shown in the inset). (c) Average specific capacities at various current rates of Mg|S cells with the CNT-S and TC-S cathode. (d) Galvanostatic charge−discharge profile for the second cycle of Mg|S cells with the CNT-S cathode (blue) and TC-S cathode (pink).

The degree of magnesium polysulfide dissolution from two different cathodes (viz. CNT-S and TC-S) was studied using UV−vis spectroscopy. Photographs of the solutions obtained following soaking of the separators in tetraglyme from CNT-S and TC-S disassembled cells at different charge/discharge voltage are shown in the inset of Figure 4 panels a and b, respectively. Differences in the solution color are observed for samples recovered from cells stopped at different depths of charge/discharge voltages. A lighter yellow color solution in the case of CNT-S indicates a lesser degree of dissolution of intermediate polysulfides compared to the TC-S cathode. As seen in Figure 4a,b, the absorbance intensities for both CNT-S and TC-S are high at discharge (1.3 V, red curve) and charge (2.5 V, pink curve). When the cell starts to discharge, the formation of higher-order polysulfides (S_8^{2-}, S_6^{2-}) takes place at 1.3 V. These higher-order polysulfides are soluble in the ether-based electrolyte and migrate from the cathode surface to the electrolyte. As a result, there is an increase in the polysulfides concentration inside the electrolyte and hence an increase in the absorbance value. Similarly, when the cell is charged to 2.5 V, lower-order polysulfide inside the cathode converts to higher-order polysulfides and migrates into the electrolyte solution. On the other hand, the intensity of absorbance is low at the final discharge (0.5 V; blue curve) and final charge (3.0 V; green curve). At the final discharge voltage (0.5 V), higher-order polysulfides convert to MgS at the cathode resulting in a decrease in the concentration of higher-order polysulfides. At the final charge voltage, the polysulfides inside the electrolyte convert to elemental sulfur, and as a result the absorbance decreases. Our findings here are like the

previously published work for the Mg|S battery.[21] Interestingly, the absorbance values in the case of CNT-S at the respective voltages are comparatively lower compared to that of the TC-S cathode. To gain additional information, the quantitative analysis of the higher-order polysulfides at various discharge/charge voltages is presented in Figure S9. Like the absorbance values, the polysulfides concentration is higher at the discharge voltage (1.3 V) and charge voltage (2.5 V) in both cases (in Figure S9c,d). However, the value is higher in the case of TC-S than CNT-S. UV−visible spectroscopy findings further support the findings from operando Raman spectroscopy. These results collectively confirm that compared to TC, the intrinsic structure of CNT is more suitable for confining sulfur and polysulfides.

The findings from operando Raman and ex-situ UV−visible spectroscopies are directly corroborated by the battery cycling results. While the TC-S represents a binder and current-collector free and self-supporting cathode material, CNT-S provides physically entrapped sulfur inside the multiwalled end-opened nanotubes (sulfur loading 82%, Figure S10) in a room temperature magnesium−sulfur (Mg|S) battery. The areal loading of sulfur (3 mg cm^{-2}) in both the cathodes are kept the same. Figure 4c demonstrates the (average) specific capacity versus current rates of the Mg|S battery for both cathode materials. The CNT-S records higher specific capacities than TC-S for the set of current densities until 1 C (1675 mA/g). The galvanostatic charge/discharge profile for the second cycle of the Mg−S cell using both of the cathodes is shown in Figure 4d. The redox process in charge/discharge matches well with the CV as shown in Figure S11. The

overpotential value is lower in the case of CNT-S (∼0.9 V; discharge and charge overpotential ≈0.5 and 0.4 V respectively with respect to OCV = 1.9 V) than TC-S (∼1.1 V; discharge and charge overpotential ≈0.6 and 0.5 V respectively with respect to OCV = 1.8 V). In the case of CNT-S, due to the entrapment of the insulating sulfur and various magnesium polysulfide intermediates inside the carbon nanotubes, the overpotential is slightly reduced. The cell assembled with CNT-S (≈ 370 mAh g^{-1} averaged over capacities for cycle numbers 10−100; first cycle = 1183 mAh g^{-1}) is nearly 1.5 times that of the TC-S (≈ 250 mAh g^{-1} averaged over capacities for cycle numbers 10−100; first cycle = 1063 mAh g^{-1}) at a current rate of 0.05 C (84 mA/g). The specific capacity for CNT-S is two times that of TC-S at 1 C. The considerable increase in the specific capacity value of the Mg|S cell using the CNT-S cathode with respect to TC-S is attributed to the successful confinement of sulfur inside the CNT, thereby reducing the dissolution of the soluble intermediate magnesium polysulfides into the liquid electrolyte solution. Electrochemical impedance spectroscopy (at 0.05 C/83.75 mA/g; Figure S12) further provides evidence in support of CNT-S as a better host than TC-S. The impedance at the 10th discharge is significantly higher for TC-S in comparison to CNT-S. This suggests that the concentration of dissolved polysulfides in the electrolyte for TC-S is higher compared to that of CNT-S with an increasing cycle number. Higher-order polysulfide dissolution in the case of the TC-S cathode results in increased viscosity and reduced conductivity of the electrolyte in the Mg|S cell leading to a higher impedance value for TC-S compared to that of CNT-S. A comparison of the battery performance of the present work with the performance of various Mg|S batteries reported recently is summarized in Figure S13.

In summary, we have convincingly shown here the importance of operando (and ex-situ) studies for mechanistic investigation of S-host/electrode characteristics and intermediates of S-electrochemistry. Operando Raman coupled with ex-situ UV−vis spectroscopic data acquired during various stages of galvanostatic discharge reveal that the intrinsic pore structure, dimensionality, and interface characteristics are some of the key design parameters for effective sulfur/polysulfide confinement, which eventually determines the battery performance. Our studies strongly reveal that CNT is more efficient than TC in confining the higher-order magnesium polysulfides. We strongly feel that this fundamental approach based on probing of dimensionally diverse model porous electrode/host systems will greatly help in unravelling the complexities of Mg chemistry and lead to the design of improved and advanced sulfur hosts with strong polysulfide confinement resulting in a superior Mg|S battery.

■ ASSOCIATED CONTENT

Ⓢⓘ Supporting Information

The Supporting Information is available free of charge at https://pubs.acs.org/doi/10.1021/acs.jpclett.1c03958.

> Experimental details, X-ray diffraction patterns of CNT and TC, Raman spectra of CNT and TC, scanning electron microscopy (SEM) images of CNT and TC, thermogravimetric analysis (TGA) of CNTS cathode, cyclic voltammograms of Mg|S cell with CNTS and TC-S cathodes, electrochemical impedance spectroscopy (EIS) of the Mg|S cell with CNT-S and TC-S as

cathodes, schematic representation of the Raman cell used for acquiring the Raman spectra and comparison with previous literature (PDF)

Transparent Peer Review report available (PDF)

■ AUTHOR INFORMATION

Corresponding Author

Aninda J. Bhattacharyya − *Solid State and Structural Chemistry Unit, Indian Institute of Science, Bengaluru 560012, India;* ⓞ orcid.org/0000-0002-0736-0004; Email: anindajb@iisc.ac.in

Authors

Ravindra Kumar Bhardwaj − *Solid State and Structural Chemistry Unit, Indian Institute of Science, Bengaluru 560012, India*

Ruth Gomes − *Solid State and Structural Chemistry Unit, Indian Institute of Science, Bengaluru 560012, India;* ⓞ orcid.org/0000-0002-8781-9283

Complete contact information is available at:
https://pubs.acs.org/10.1021/acs.jpclett.1c03958

Author Contributions

#R.K.B. and R.G. contributed equally to this work.

Notes

The authors declare no competing financial interest.

■ REFERENCES

(1) Larcher, D.; Tarascon, J. M. Towards Greener and More Sustainable Batteries for Electrical Energy Storage. *Nat. Chem.* **2015**, 7 (1), 19−29.

(2) Dunn, B.; Kamath, H.; Tarascon, J. M. Electrical Energy Storage for the Grid: A Battery of Choices. *Science* **2011**, 334 (6058), 928−935.

(3) Armand, M.; Tarascon, J. Building Better Batteries. *Nature* **2008**, 451, 652−657.

(4) Kalyanasundaram, K.; Grätzel, M. Themed Issue: Nanomaterials for Energy Conversion and Storage. *J. Mater. Chem.* **2012**, 22 (46), 24190−24194.

(5) Goodenough, J. B.; Park, K. S. The Li-Ion Rechargeable Battery: A Perspective. *J. Am. Chem. Soc.* **2013**, 135 (4), 1167−1176.

(6) Evers, S.; Nazar, L. F. New Approaches for High Energy Density Lithium−Sulfur Battery Cathodes. *Acc. Chem. Res.* **2013**, 46 (5), 1135−1143.

(7) Ji, X.; Lee, K. T.; Nazar, L. F. A Highly Ordered Nanostructured Carbon−Sulphur Cathode for Lithium−Sulphur Batteries. *Nat. Mater.* **2009**, 8 (6), 500−506.

(8) Manthiram, A.; Fu, Y.; Chung, S.-H.; Zu, C.; Su, Y.-S. Rechargeable Lithium−Sulfur Batteries. *Chem. Rev.* **2014**, 114 (23), 11751−11787.

(9) Kim, H. S.; Arthur, T. S.; Allred, G. D.; Zajicek, J.; Newman, J. G.; Rodnyansky, A. E.; Oliver, A. G.; Boggess, W. C.; Muldoon, J.

Structure and Compatibility of a Magnesium Electrolyte with a Sulphur Cathode. *Nat. Commun.* **2011**, *2* (1). DOI: 10.1038/ncomms1435

(10) Guo, Y. S.; Zhang, F.; Yang, J.; Wang, F. F.; Nuli, Y.; Hirano, S. I. Boron-Based Electrolyte Solutions with Wide Electrochemical Windows for Rechargeable Magnesium Batteries. *Energy Environ. Sci.* **2012**, *5* (10), 9100−9106.

(11) Huie, M. M.; Bock, D. C.; Takeuchi, E. S.; Marschilok, A. C.; Takeuchi, K. J. Cathode Materials for Magnesium and Magnesium-Ion Based Batteries. *Coord. Chem. Rev.* **2015**, *287*, 15−27.

(12) Schwarz, R.; Pejic, M.; Fischer, P.; Marinaro, M.; Jörissen, L.; Wachtler, M. Magnesocene-Based Electrolytes: A New Class of Electrolytes for Magnesium Batteries. *Angew. Chemie - Int. Ed.* **2016**, *55* (48), 14958−14962.

(13) Ji, X.; Lee, K. T.; Nazar, L. F. A Highly Ordered Nanostructured Carbon-Sulphur Cathode for Lithium-Sulphur Batteries. *Nat. Mater.* **2009**, *8* (6), 500−506.

(14) Tutusaus, O.; Mohtadi, R. Paving the Way towards Highly Stable and Practical Electrolytes for Rechargeable Magnesium Batteries. *ChemElectroChem.* **2015**, *2* (1), 51−57.

(15) Muldoon, J.; Bucur, C. B.; Oliver, A. G.; Sugimoto, T.; Matsui, M.; Kim, H. S.; Allred, G. D.; Zajicek, J.; Kotani, Y. Electrolyte Roadblocks to a Magnesium Rechargeable Battery. *Energy Environ. Sci.* **2012**, *5* (3), 5941−5950.

(16) Saha, P.; Datta, M. K.; Velikokhatnyi, O. I.; Manivannan, A.; Alman, D.; Kumta, P. N. Rechargeable Magnesium Battery: Current Status and Key Challenges for the Future. *Prog. Mater. Sci.* **2014**, *66*, 1−86.

(17) Song, J.; Sahadeo, E.; Noked, M.; Lee, S. B. Mapping the Challenges of Magnesium Battery. *J. Phys. Chem. Lett.* **2016**, *7* (9), 1736−1749.

(18) Kumar, N.; Siegel, D. J. Interface-Induced Renormalization of Electrolyte Energy Levels in Magnesium Batteries. *J. Phys. Chem. Lett.* **2016**, *7* (5), 874−881.

(19) Bucur, C. B.; Gregory, T.; Oliver, A. G.; Muldoon, J. Confession of a Magnesium Battery. *J. Phys. Chem. Lett.* **2015**, *6* (18), 3578−3591.

(20) Gao, T.; Noked, M.; Pearse, A. J.; Gillette, E.; Fan, X.; Zhu, Y.; Luo, C.; Suo, L.; Schroeder, M. A.; Xu, K.; Lee, S. B.; Rubloff, G. W.; Wang, C. Enhancing the Reversibility of Mg/S Battery Chemistry through Li$^+$ Mediation. *J. Am. Chem. Soc.* **2015**, *137* (38), 12388−12393.

(21) Yu, X.; Manthiram, A. Performance Enhancement and Mechanistic Studies of Magnesium-Sulfur Cells with an Advanced Cathode Structure. *ACS Energy Lett.* **2016**, *1* (2), 431−437.

(22) Robba, A.; Vizintin, A.; Bitenc, J.; Mali, G.; Arčon, I.; Kavčič, M.; Žitnik, M.; Bučar, K.; Aquilanti, G.; Martineau-Corcos, C.; Randon-Vitanova, A.; Dominko, R. Mechanistic Study of Magnesium-Sulfur Batteries. *Chem. Mater.* **2017**, *29* (21), 9555−9564.

(23) Gao, T.; Ji, X.; Hou, S.; Fan, X.; Li, X.; Yang, C.; Han, F.; Wang, F.; Jiang, J.; Xu, K.; Wang, C. Thermodynamics and Kinetics of Sulfur Cathode during Discharge in MgTFSI$_2$−DME Electrolyte. *Adv. Mater.* **2018**, *30* (3), 1704313.

(24) Bieker, G.; Wellmann, J.; Kolek, M.; Jalkanen, K.; Winter, M.; Bieker, P. Influence of Cations in Lithium and Magnesium Polysulphide Solutions: Dependence of the Solvent Chemistry. *Phys. Chem. Chem. Phys.* **2017**, *19* (18), 11152−11162.

(25) Nakayama, Y.; Matsumoto, R.; Kumagae, K.; Mori, D.; Mizuno, Y.; Hosoi, S.; Kamiguchi, K.; Koshitani, N.; Inaba, Y.; Kudo, Y.; Kawasaki, H.; Miller, E. C.; Weker, J. N.; Toney, M. F. Zinc Blende Magnesium Sulfide in Rechargeable Magnesium-Sulfur Batteries. *Chem. Mater.* **2018**, *30* (18), 6318−6324.

(26) Yeon, J.-T.; Jang, J.-Y.; Han, J.-G.; Cho, J.; Lee, K. T.; Choi, N.-S. Raman Spectroscopic and X-Ray Diffraction Studies of Sulfur Composite Electrodes during Discharge and Charge. *J. Electrochem. Soc.* **2012**, *159* (8), A1308−A1314.

(27) Hagen, M.; Schiffels, P.; Hammer, M.; Dörfler, S.; Tübke, J.; Hoffmann, M. J.; Althues, H.; Kaskel, S. In-Situ Raman Investigation of Polysulfide Formation in Li-S Cells. *J. Electrochem. Soc.* **2013**, *160* (8), A1205−A1214.

(28) Diao, Y.; Xie, K.; Xiong, S.; Hong, X. Insights into Li-S Battery Cathode Capacity Fading Mechanisms: Irreversible Oxidation of Active Mass during Cycling. *J. Electrochem. Soc.* **2012**, *159* (11), A1816−A1821.
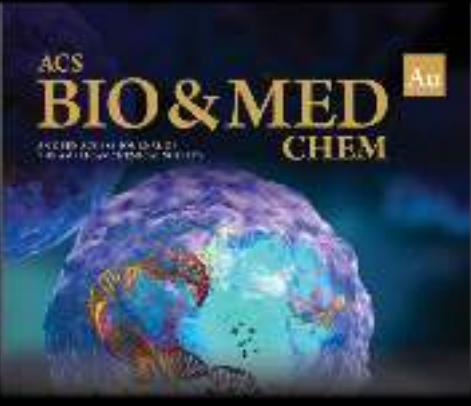
(29) Bhardwaj, R. K.; Jayanthi, S.; Adarakatti, P. S.; Sood, A. K.; Bhattacharyya, A. J. Probing the Extent of Polysulfide Confinement Using a CoNi$_2$S$_4$Additive Inside a Sulfur Cathode of a Na/Li-Sulfur Rechargeable Battery. *ACS Appl. Mater. Interfaces* **2020**, *12* (25), 28120−28128.

(30) Zhu, W.; Paolella, A.; Kim, C. S.; Liu, D.; Feng, Z.; Gagnon, C.; Trottier, J.; Vijh, A.; Guerfi, A.; Mauger, A.; Julien, C. M.; Armand, M.; Zaghib, K. Investigation of the Reaction Mechanism of Lithium Sulfur Batteries in Different Electrolyte Systems by: In Situ Raman Spectroscopy and in Situ X-Ray Diffraction. *Sustain. Energy Fuels* **2017**, *1* (4), 737−747.

(31) Wu, H. L.; Huff, L. A.; Gewirth, A. A. In Situ Raman Spectroscopy of Sulfur Speciation in Lithium-Sulfur Batteries. *ACS Appl. Mater. Interfaces* **2015**, *7* (3), 1709−1719.

(32) Hannauer, J.; Scheers, J.; Fullenwarth, J.; Fraisse, B.; Stievano, L.; Johansson, P. The Quest for Polysulfides in Lithium-Sulfur Battery Electrolytes: An Operando Confocal Raman Spectroscopy Study. *ChemPhysChem* **2015**, *16* (13), 2755−2759.

(33) Chen, J.-J.; Yuan, R.-M.; Feng, J.-M.; Zhang, Q.; Huang, J.-X.; Fu, G.; Zheng, M.-S.; Ren, B.; Dong, Q.-F. Conductive Lewis Base Matrix to Recover the Missing Link of Li$_2$S$_8$ during the Sulfur Redox Cycle in Li-S Battery. *Chem. Mater.* **2015**, *27* (6), 2048−2055.